Point-to-point responses

We appreciate the reviewers for their valuable and constructive comments, which are very helpful for the improvement of the manuscript. We have revised the manuscript carefully according to the reviewers' comments. We have addressed the reviewers' comments on a point-to-point basis as below for consideration, where the reviewers' comments are cited in ***black****, and the responses are in* ***blue****.*

Referee #1

The authors have provided a detailed response to the original two referees and in particular the error budget, underlying DOAS fits, and TUV model set up to determine OH production are now much more clear. They have also provided further support for near surface ozone and transport of ozone and NO_x to the site. These provide good support for some of their key results near the surface which are most results reported in the abstract. However, questions particular to the vertical profiles remain which could indirectly still impact the key results.

I have two major comments:

1. What is the information content of the retrieved profiles? Can the authors provide representative or average values for averaging kernels (AVK) or degrees of freedom (DOF) for specific altitudes? The authors report that results with less than 1 DOF are filtered, but this will typically be concentrated near the surface. In Fig. 4 results are shown as high as 1.8 km agl. and in in Figs. 5 and 7 to 4 km agl. Are the results at higher altitudes significant or simply conforming to the a priori? Information is needed to assess this.

Re. Many thanks for your great comments.

(1) The information content for vertical profile quality control includes: cloud information, retrieval error, averaging kernel (AVK, sensitivity to different altitudes), degrees of freedom (DOF, trace of the averaging kernel matrix), and cost function. The information content for the retrieved profiles include: vertical profiles, averaging kernels, gain, retrieval errors, weighting function, cost function (Chisquare), degree of freedom for signal, retrieved VCDs and the corresponding errors.

(2) The average averaging kernels (AVK) and degree of freedom (DOF) for aerosol, H_2O, NO_2, HONO and O_3 were shown in Figure R1.

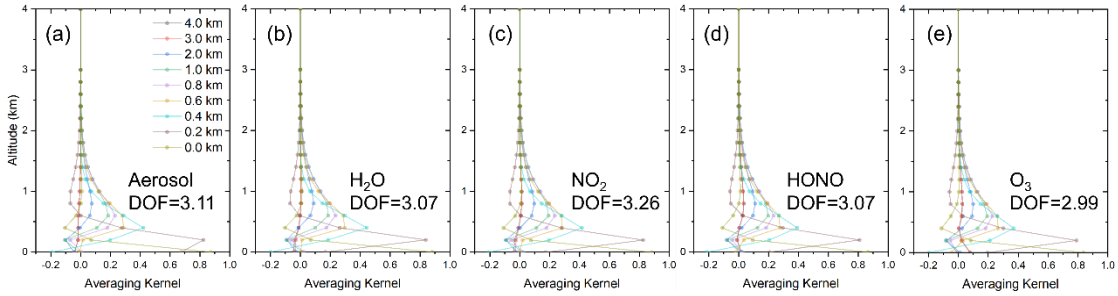

Figure R1. The average AVK and DOF of the retrieved aerosol (a), H_2O (b), NO_2 (c), HONO (d) and O_3 (e), respectively.

The average AVK and DOF in our study is at the same level as previous studies (Bosch et al., 2018; Friess et al., 2019). AVK denotes the sensitivity of the retrieval at different heights and DOF denotes the trace of the AVK matrix. From the above results, we can also find that the retrieval results have sensitivity at high altitude, even 4 km.

(3) In our study, we used a combination of observation and gain iterations, net of the algorithm's dependence on a priori profile. Therefore, the retrieved results are independent of the a priori profiles, and it only act as an intermediate variable in the iterative process.

(4) In this study, we estimated the contribution of different error sources to the AOD and VCDs of trace gases, and near-surface (0–200 m) trace gases' concentrations and aerosol extinction coefficients (AECs), respectively. The detailed demonstrations and estimation methods are displayed below, and the corresponding varies errors are summarized in Table 1.

a. Smoothing errors arise from the limited vertical resolution of profile retrieval. Noise errors denote the noise in the spectra (i.e., the error of DOAS fits). Considering the error of the retrieved state vector equaling the sum of these two independent errors, we calculated the sum of smoothing and noise errors on near-surface concentrations and column densities, which were 13 and 5 % for aerosols, 13 and 36 % for H_2O, 12 and 14 % for NO_2, 18 and 21 % for HONO, and 12 and 32 % for O_3, respectively.
b. Algorithm error is denoted by the differences between the measured and simulated DSCDs. This error contains forward model error from an imperfect approximation of forward function, parameter error of forward model, and other errors, such as detector noise (Rodgers, 2004). Algorithm error is a function of the viewing angle, and it is difficult to assign this error to each altitude. Thus, this error on the near-surface values and column densities is estimated through calculating the average relative differences between the measured and simulated DSCDs at the minimum and maximum elevation angle (except 90°), respectively (Wagner et al., 2004). In this study, we estimated these errors on the near-surface values and the column densities at 4 and 8 % for aerosols, 3 and 11 % for NO_2, and 20 and 20 % for HONO referring to Wang et al. (2017, 2020), 1 and 8 % for H_2O referring to Lin et al. (2020), and 6 and 10 % for O_3 referring to Ji et al. (2023), respectively.
c. Cross section error arises from the uncertainty in the cross section. According to Thalman and Volkamer, (2013), Lin et al. (2020), Vandaele et al. (1998), Stutz et al. (2000), and Serdyuchenko et al. (2014), we adopted 4, 3, 3, 5, and 2 % for O_4 (aerosols), H_2O, NO_2, HONO and O_3, respectively.
d. The profile retrieval error for trace gases is sourced from the uncertainty of aerosol extinction profile retrieval and propagated to trace gas profile. This error could be roughly estimated based on a linear propagation of the total error budgets of the aerosol retrievals. The errors of the learned four trace gases were roughly estimated at 14 % for VCDs and 10 % for near-surface concentrations, respectively.

The total uncertainty was the sum of all above errors in the Gaussian error propagation, and the error results were listed in Table 1. We found that the smoothing and noise errors played a dominant role in the total uncertainties of aerosol and trace gases. Moreover, improving the accuracy and temperature gradient of the absorption cross

section is another important means to reduce the uncertainty of the vertical profiles in the future, especially for O_3.

Table 1. Error budget estimation (in %) of the retrieved near-surface (0–200 m) concentrations of trace gases and AECs, and AOD and VCDs.

		Error sources				Total
		Smoothing and noise errors	Algorithm error	Cross section error	Related to the aerosol retrieval (only for trace gases)	
Near-surface	aerosol	13	4	4	-	14
	H_2O	13	1	3	14	19
	NO_2	12	3	3	14	18
	HONO	18	20	5	14	29
	O_3	12	6	2	14	19
VCD or AOD	AOD	5	8	4	-	10
	H_2O	36	8	3	10	38
	NO_2	14	11	3	10	20
	HONO	21	20	5	10	31
	O_3	32	10	2	10	35

Certainly, we also did independent validations. However, there was not other vertical observations during our campaign on the TP. Therefore, we did validations between in situ measurements and the bottom layer of MAX-DOAS profiles (Figure R2).

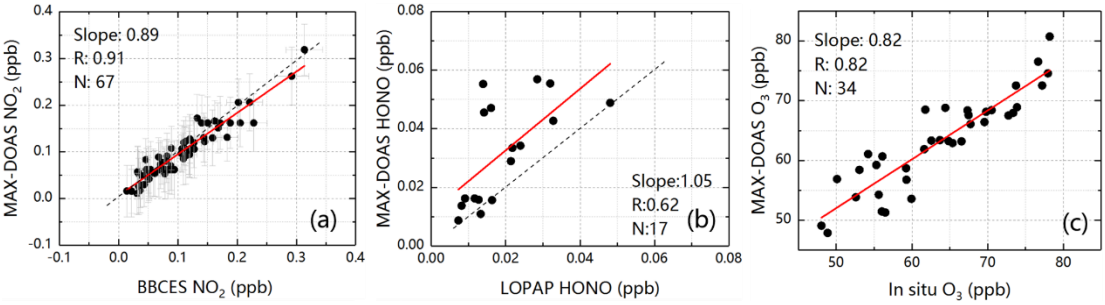

Figure R2. Validations of (a) MAX-DOAS NO_2 vs in situ NO_2, (b) MAX-DOAS HONO vs LOPAP HONO, (c) MAX-DOAS O_3 vs in situ O_3.

Moreover, we did vertical-profile validations in Shanghai and Beijing. As shown in Figure R3, we used Mie lidar to validate MAX-DOAS aerosol vertical profiles, and used balloon-based NO_2 profiles to validate MAX-DOAS NO_2 vertical profiles (Xing et al., 2017). The good agreement indicates the reliability of MAX-DOAS retrieved aerosol and NO_2 profiles.

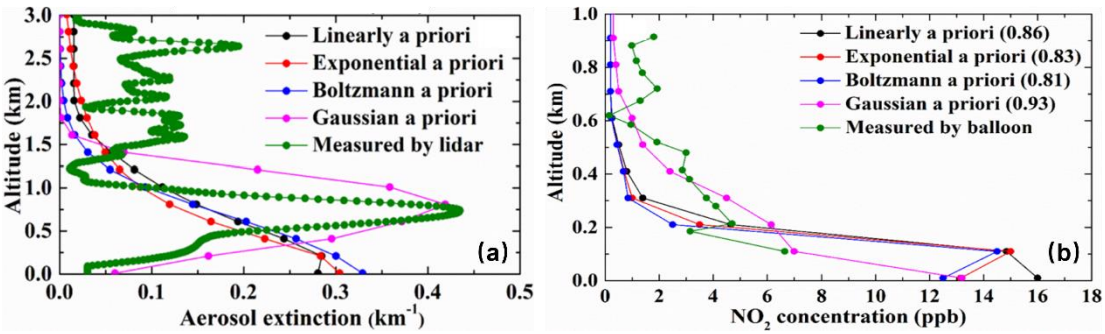

Figure R3. Validations of (a) MAX-DOAS aerosol profile vs lidar aerosol profile, (b) MAX-DOAS NO_2 profile vs balloon-based NO_2 profile.

(5) Finally, the intercomparison of HONO results during CINDI-2 campaign reported by Thomas Wagner's group revealed "Another interesting finding for the "EnviMes" instruments is that although the same set of spectra measured by the "USTC" instruments is analysed by the "DLR" and "USTC" researchers, much larger rms values and fit errors are found for the "DLR(1)" and "DLR(2)" results (especially for the "DLR(2) " results with the "sequential FRS") than for the "USTC(1)" and "USTC(2)". (Wang et al., 2020)"

2. More information is still needed regarding the calculation of and reporting of results related to OH production.

a. Firstly, the authors state in the abstract "O_3 and HONO were the main contributors to OH on the TP" and have similar language to this effect in the main text, however, they do not appear to consider other sources. This is therefore not a finding and the language should reflect that.

Re. Many thanks for your great comments.

As reported in previous studies, the precursors of OH on the Tibetan Plateau were O_3, HONO, NO_2 and HCHO (Lin, et al., 2008; Xing, et al., 2021; Lyu, et al., 2020; Zhang, et al., 2021; Wang, et al., 2023). While considering the low background concentration of NO_2 and HCHO, and their pathways to produce OH, the contribution to OH of NO_2 and HCHO than HONO and O_3 is lower (Sörgel, et al., 2011).

Moreover, we have modified our description as following:

(1) That indicated O_3 was an important contributor of OH production (> 80%) on the TP, which was about 5-6 times to HONO.

(2) O_3 and HONO were important source of OH on the TP.

b. Related to major comment 1, O_3 and H_2O appear to be sometimes or always elevated at high altitudes relative to other retrieved species potentially driving the resulting OH source.

i. O_3 appears to never drop below 48 ppb, is this based on the a priori or is it retrieved? If it is from the a priori why is O_3 given a non-zero concentration it decays to when other species are not. Is it based on TROPOMI or lidar data in Fig. S4 if so that needs to be explicit? These would seem to leave room for substantial variability in the free tropospheric background. I will also note that the various traces in Fig. S4 are not explained and units are not the same across panels.

Re. Many thanks for your great comments.

The vertical profiles in Figure 5 (e) of the manuscript were averaged profiles. Figure R4 showed the hourly variations of surface ozone during all the observation period. The minimum and maximum concentrations of the surface O_3 were 29.65 ppb and 162.37 ppb, respectively.

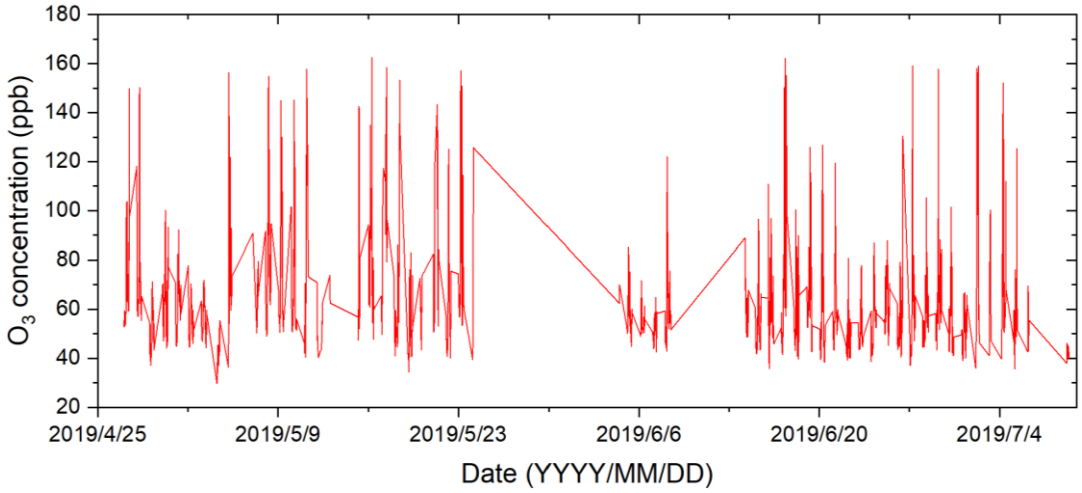

Figure R4. Variations of surface O_3 concentrations from 27 April to 09 July 2019.

Another fact that we need to account for is that we only observed O_3 variations during the daytime. For the retrieval algorithm, aiming at the bottleneck of strong absorption interference in the stratosphere, which makes it difficult to realize O_3 profile retrieval by ground-based MAX-DOAS alone, a joint satellite-ground based hyperspectral remote sensing algorithm was developed. Reduction of stratospheric O_3 absorption interference by 80-90% by coupling hyperspectral satellite remote sensing of stratospheric O_3 profiles. Moreover, we have solved the problem of insufficient sensitivity of ground-based MAX-DOAS to high-altitude O_3 by coupling satellite remote sensing tropospheric O_3 observations to build an inverse a priori profile dataset (Ji et al., 2023). Therefore, the retrieved results are independent of the a priori profiles, and it only act as an intermediate variable in the iterative process. We have also validated the retrieved O3 profiles with tower-based in-situ measurements (Figure R5).

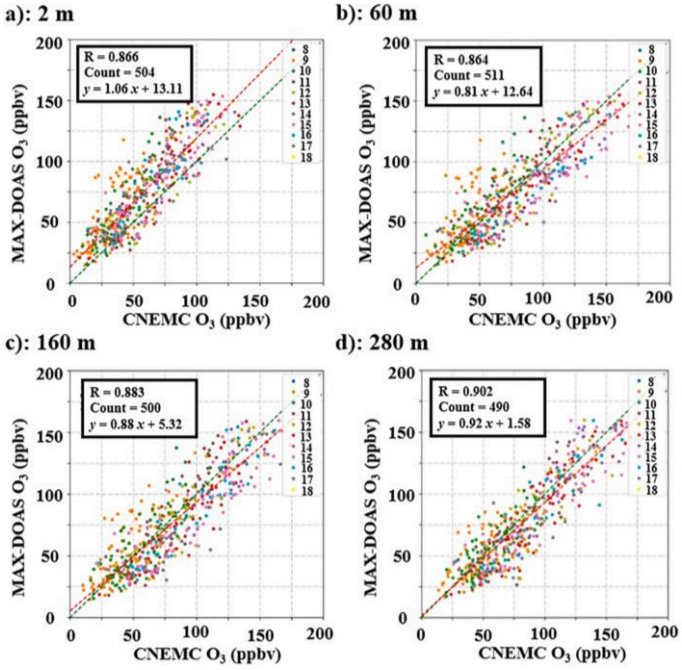

Figure R5. Linear regression plots for O_3 comparison results at different altitudes; IAP site (a) MAX-DOAS 0-100 m layer vs 2 m in tower; (b) MAX-DOAS 0-100 m layer vs 60 m in tower; (c) MAX-DOAS 100-200 m layer vs 160 m in tower; (d) MAX-

DOAS 200-300 m layer vs 280 m in tower.

The retrieved results depended on the true concentration of atmospheric species in the atmosphere and the corresponding detection limits of the instrument. The detection limit can be quantified as following:

$$\overline{D}_{limit} \approx \sigma \times \frac{6}{\sqrt{n-1}}$$

Where, n and σ were the number of channels and noise level of the spectrometer, respectively. The detection limits of aerosol, H_2O, NO_2, HONO and O_3 were shown in Table 2.

Table 2. Detection limit of our instrument.

	Detection limits
Aerosol	0.05 km^{-1}
H_2O	0.05%
NO_2	0.1 ppb
HONO	0.1 ppb
O_3	0.1 ppb

Figure S4 depicted the diurnal variation of PBL height, which was calculated using aerosol vertical profiles to calculate the heights with fastest variation rates of aerosols. We have also validated the calculated PBL with WRF simulated PBL.

Figure S8 showed the O_3 vertical profiles measured by TROPOMI at Nam Co, lidar at Yangbajing, ozonesonde at Qaidam, and lidar at Lhasa. These data and figures were all from previous researches. The purpose of referring these studies was only to elucidate that the exponential decreasing vertical profile shape of O_3 below 1 km in the Nam Co region is reasonable.

ii. H_2O appears to frequently increase above ~3 km agl, sometimes to concentrations greater than at the surface despite presumably lower temperatures and pressures at those altitudes. Is this allocation of the remaining column being placed at high altitudes or actually localized at the higher altitudes?

Re. Many thanks for your great comments.

Firstly, we only retrieved the vertical profiles on sunny and cloud-free periods. The influence of cloud can be filtered.

Secondly, the accuracy of the H_2O vertical profile algorithm has been validated at another station (Beijing) as following.

Three representative water vapor profiles were retrieved from the MAX-DOAS measurements taken on three clear days: (a) 0 May 2018; (b) 19 June 2018; and (c) 31 July 2018; these were validated with the corresponding ballon-borne radiosonde profiles, as shown in Figure R6. The surface concentrations of these representative profiles are located in different concentration ranges. The ballon-borne radiosonde data were interpolated onto the MAX-DOAS grid for comparison. Furthermore, the interpolated ECMWF ERA-interim profiles were also used to validate the MAX-DOAS profiles. The correlation analysis results for the MAX-DOAS profiles and corresponding balloon-borne radiosonde profiles are displayed in the bottom panels of Figure R6, where the colors represent the height of each layer and horizontal gray lines

indicate the errors of retrieved profile in different height layers. The biases and standard deviations between MAX-DOAS profiles and corresponding balloon-borne radiosonde profiles on 8 May 2018; 19 June 2018; and 31 July 2018 are $-0.14\pm1.78\times10^{16}$, $-0.51\pm3.10\times10^{16}$, and $-1.10\pm4.36\times10^{16}$. Here, all values are in units of molec/cm^3. Overall, the water vapor profiles retrieved from MAX-DOAS and radiosonde measurements exhibit a high level of consistency, with high Pearson correlation coefficients (R) for these three profiles.

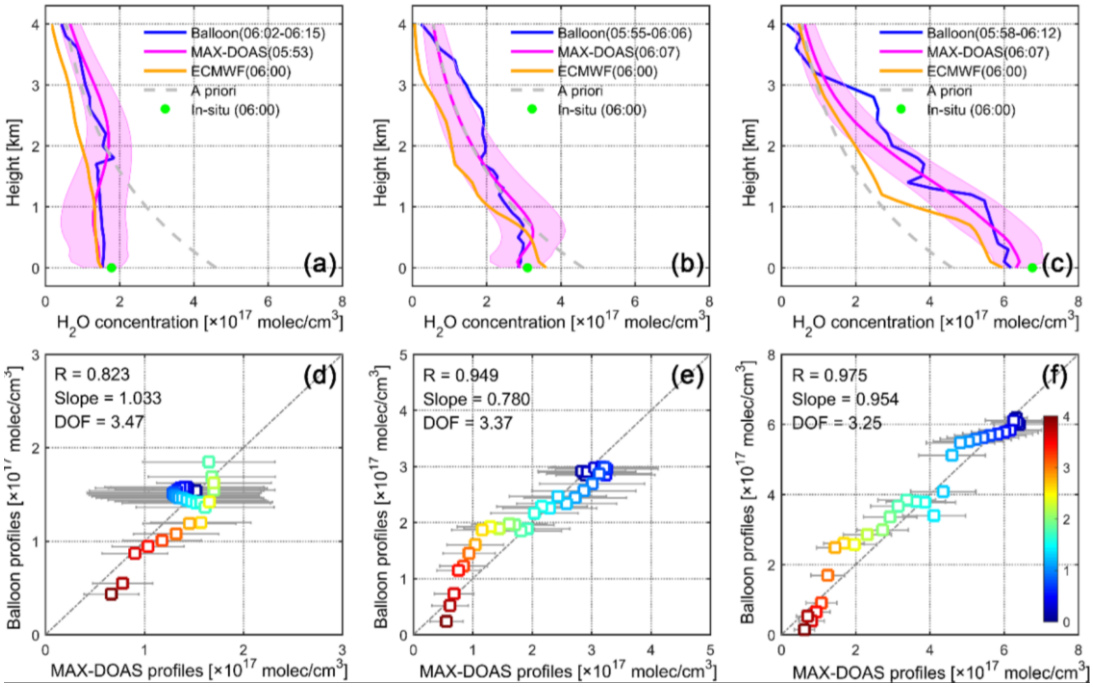

Figure R6. Three typical water vapor profiles retrieved from MAX-DOAS with the corresponding balloon-borne radiosonde measurements, ECMWF ERA-interim datasets, and NCDC in-situ measurements taken on 8 May 2018 (a); 19 June 2018 (b); and 31 July 2018 (c). The blue lines represent the water vapor concentration profiles measured by balloon-borne radiosonde. The pink lines and the shaded areas represent the MAX-DOAS retrieved water vapor profiles and their errors. The orange lines represent the water vapor profiles derived from the ECMWF ERA-interim reanalysis dataset. The dashed gray lines represent the a priori profile used in water vapor profile retrieval. The green dots represent the surface concentration of water vapor measured by the NCDC in-situ instruments. The bottom panels display the corresponding correlation analysis results between the MAX-DOAS-retried and radiosonde water vapor profiles on 8 May (a); 19 June 2018 (b); and 31 July 2018 (f), where colors indicate the height of each layer and the horizontal gray lines indicate the errors of retrieved profile in different height layers.

As shown in Figure R7, we conducted a correlation analysis of the water vapor concentrations in different height layers (derived from the MAX-DOAS and ECMWF ERA-interim data) to validate the profiles. As performed for the balloon-borne radiosonde measurements, the ECMWF ERA-interim water vapor profiles were also interpolated onto the MAX-DOAS grid. During this observation period, the MAX-DOAS instruments collected spectra from 00:00 to 10:00 (UTC). However, the

temporal resolution of the ECMWF ERA-interim dataset is 6 h. Thus, only the MAX-DOAS profiles measured at 00:00 and 06:00 can be used to validate the corresponding ECMWF profiles. These validations were conducted under no-cloud conditions by synchronizing the timetable to the AERONET data. In total, 138 profiles measured with MAX-DOAS in this observation period from 18 April to 30 September 2018 were validated using the coincident ECMWF profiles.

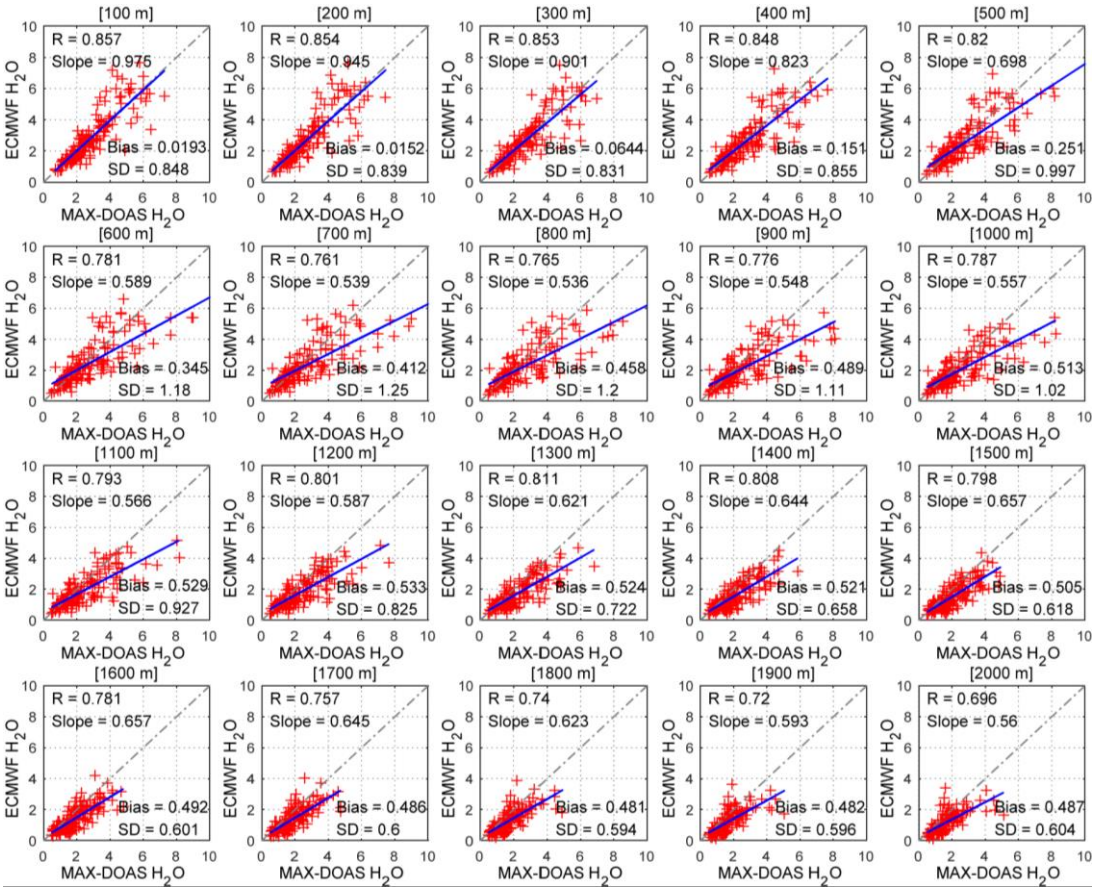

Figure R7. Correlation analysis of MAX-DOAS water vapor concentrations and ECMWF results in different the MAX-DOAS grid using a linear method to facilitate vertical layers. The 00:00 and 06:00 UTC ECMWF profiles are interpolated onto the comparison. Both the MAX-DOAS and ECWMF profiles are normalized to the AERONET timetable for cloud screening. The Pearson correlation coefficient (R), linear fitting slope (Slope), the bias with stand deviation (SD) between MAX-DOAS and ECMWF result as each layer are given in this figure. All values here are in units of 10^{17} molec/cm^2.

Good agreement between the MAX-DOAS and ECMWF results can be observed in height layers below 2000 m, with the Pearson correlation coefficient (R) ranging from 0.695 to 0.857. Under an increase in layer heigh, the detection sensitivity of MAX-DOAS gradually decreases and the correlation analysis results degrade. In the layer height from 600 to 1200 m, the consistency between the MAX-DOAS concentrations and the ECMWF results in slightly worse, which may be the result of the large uncertainties in these layers. The decreasing detection sensitivity and the enhances constraint of a priori profile together lead to the decreasing linear fitting slope with

increasing height. MAX-DOAS results have high sensitivities in the lower atmosphere and the contribution of a priori profile in retrieved profile is relatively small. With the increasing height, the detection sensitivity gets worse and the dependence of retrieved profile in a priori profile becomes strong gradually. The fixed exponentially decreasing a priori profile with a surface concentration of 4.6×10^{17} molec/cm^3 and a scale height of 1.9 km may be too high to represent the water vapor concentration in high altitudes. Together with the low sensitivity in high altitudes, the retrieved concentrations in high altitudes can be higher than actual situation, thus the linear fitting slope decreases and the bias between MAX-DOAS and ECMWF increases, as shown in Figure R7.

Zhang et al. (2013) also reported that the water vapor concentration gradually increases from low to high altitudes below 6000 m, and peaks at 5000 m-6000 m, during the Indian Ocean monsoon (Figure R8). Moreover, the water vapor transport direction is from southwest to northeast, which corresponds to the direction of the Indian Ocean monsoon.

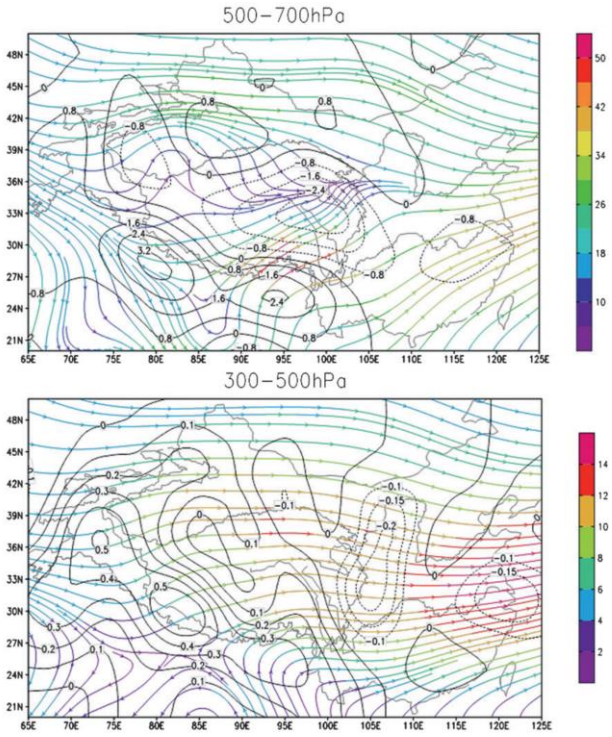

Figure R8. Water vapor flux (streamlines; kg m^{-1} s^{-1}) and divergence of moisture flux (contours; 10^{-5} kg m^{-2} s^{-1}) for (top) 500-700 hPa and (middle) 300-500 hPa during the warm season.

Therefore, we believe that high-altitude water vapor on the Tibetan Plateau during the observation period is plausible.

iii. The TP is a frequent site of stratospheric intrusions (Škerlak et al., 2015) as has been observed at Nam Co in particular (Yin et al., 2017) one would expect this to drive greater profile variability for O_3 and H_2O (and possibly other gases) is this hiding in the averages or is there a reason it is not detected? If there are high-O_3 and low H_2O air masses descending over the site will that impact the retrieval?

Re. Many thanks for your great comments.

The spatial resolution of vertical profiles was 100 m. The temporal resolution of vertical profiles was less than 15 min. Based on this spatiotemporal resolution, it is possible to capture pollutants if they are transported from high altitude to near surface. Moreover, different pollutants have different spectral absorption structures (absorption cross sections), and in our algorithm there is little interaction between each species.

In this study, we can't find that O_3 transport from high altitude to ground surface. But, we found the transport process of H_2O at higher altitudes, such as 17 May, 18 May, 23 May, and 30 June 2019 (Figure R9).

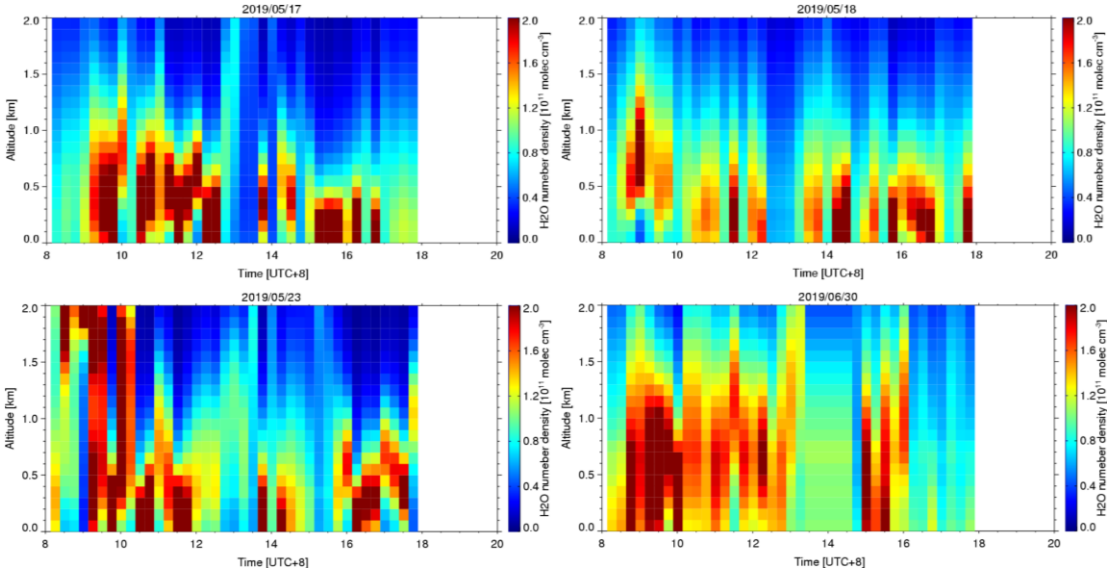

Figure R9. Diurnal variations of vertical profiles of H_2O on 17 May, 18 May, 23 May, and 30 June 2019.

c. The authors have provided a detailed response regarding their implementation of TUV already, but can they address how uncertainty in the retrieved profiles might impact the TUV calculations?

Re. Many thanks for your great comments.

Previous studies reported the that the simulated actinic flux was larger 10%-40% than the measured actinic flux on clear and cloud-free days (Koepke et al., 1998; Badosa et al., 2005; Palancar et al., 2013; Ryu et al., 2017).

In this study, we used online TUV model.

https://www2.acom.ucar.edu/modeling/tropospheric-ultraviolet-and-visible-tuv-radiation-model

The main parameters for this model were cloud information, total ozone column, aerosol optical depth (AOD), single scattering albedo (SSA), and Ångström exponents. In this study, we selected clean and cloud free days, the AOD at 361 nm was derived from aerosol extinction profiles measured by MAX-DOAS; the daily total ozone column density was measured by TROPOMI with a value range of 260-280 DU; the single scattering albedo (SSA) was calculated based on the regression analysis of multi-wavelength (361 and 477 nm) O_4 absorptions measured by MAX-DOAS (Xing et al., 2019); fixed Ångström exponents of 0.508, 0.581 and 0.713 were used in May, June and July, respectively, referring to Xia et al. (2011).

The parameter scheme and the corresponding code of TUV model can be found at: *https://www2.acom.ucar.edu/modeling/tuv-download*

As shown in Figure R10, when we put cloud information, total ozone column, aerosol optical depth (AOD), single scattering albedo (SSA), and Ångström exponents into the TUV model, the uncertainty of simulated actinic flux can decreased significantly (5%-9%).

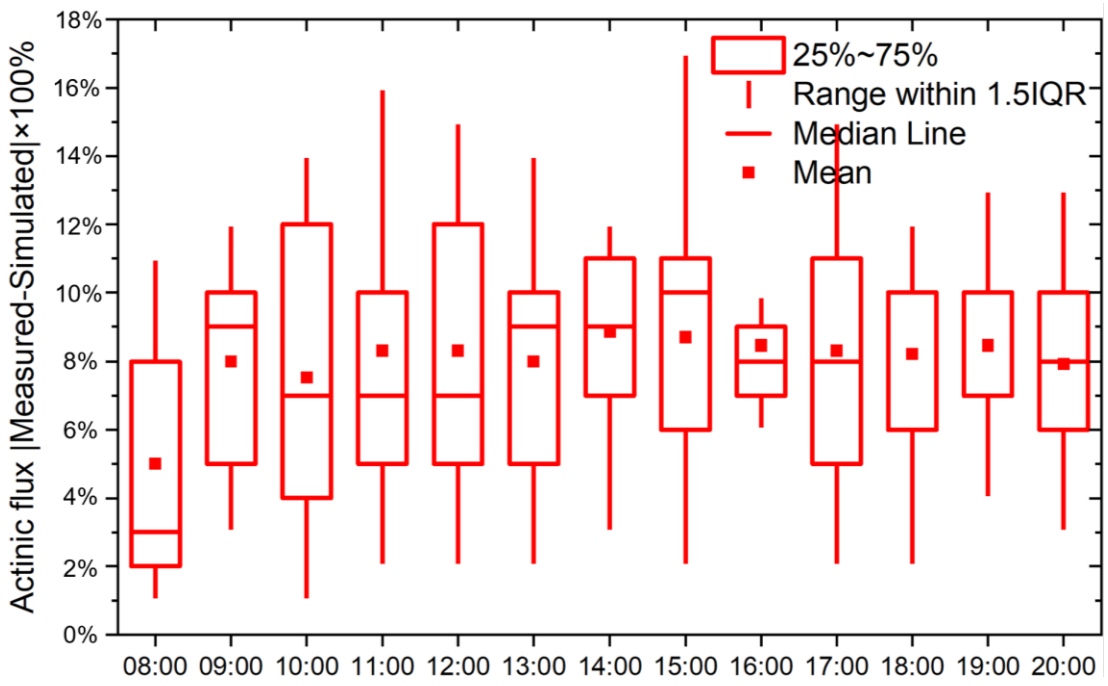

Figure R10. |Measured actinic flux-TUV simulated actinic flux|×100%

In addition, the calculated OH were validated with measured OH, but the specific discussion will be organized in a separate study.

References:

[1] Škerlak, B., Sprenger, M., Pfahl, S., Tyrlis, E., and Wernli, H.: Tropopause folds in ERAInterim: Global climatology and relation to extreme weather events, Journal of Geophysical Research: Atmospheres, 120, 4860–4877, https://doi.org/10.1002/2014JD022787, 2015.

[2] Yin, X., Kang, S., De Foy, B., Cong, Z., Luo, J., Zhang, L., Ma, Y., Zhang, G., Rupakheti, D., and Zhang, Q.: Surface ozone at Nam Co in the inland Tibetan Plateau: Variation, synthesis comparison and regional representativeness, Atmos Chem Phys, 17, 11293– 11311, https://doi.org/10.5194/ACP-17-11293-2017, 2017.

[3] Lin, H., Liu, C., Xing, C., Hu, Q., Hong, Q., Liu, H., Li, Q., Tan, W., Ji, X., Wang, Z., and Liu, J.: Validation of water vapor vertical distributions retrieved from MAX-DOAS over Beijing, China, Remote Sens., 12, 3193, https://doi.org/10.3390/rs12193193, 2020.

[4] Zhang, Y., Wang, D., Zhai, P., Gu, G., and He, J.: Spatial distributions and seasonal variations of tropospheric water vapor content over the Tibetan Plateau, J. Climate, 26, 15, 5637-5654, https://doi.org/10.1175/JCLI-D-12-00574.1, 2013.

[5] Ji, X., Liu, C., Wang, Y., Hu, Q., Lin, H., Zhao, F., Xing, C., Tang, G., Zhang, Q., and Wagner, T.: Ozone profiles without blind area retrieved from MAX-DOAS measurements and comprehensive validation with multi-platform observations, Remote Sens. Environ., 284, 113339, https://doi.org/10.1016/j.rse.2022.113339, 2023.

[6] Lin, W., Zhu, T., Song, Y., Zou, H., Tang, M., Tang, X., and Hu, J.: Photolysis of surface O_3 and production potential of OH radicals in the atmosphere over the Tibetan Plateau, J. Geophys. Res.-Atmos., 113, D02309, doi:10.1029/2007JD008831, 2008.

[7] Xing, C., Liu, C., Wu, H., Lin, J., Wang, F., Wang, S., and Gao, M.: Ground-based vertical profile observations of atmospheric composition on the Tibetan Plateau (2017-2019), Earth Syst. Sci. Data, 13, 4897-4912, https://doi.org/10.5194/essd-13-4897-2021, 2021.

[8] Lyu, X., Guo, H., Zhang, W., Cheng, H., Yao, D., Lu, H., Zhang, L., Zeren, Y., Liu, X., Qian, Z., and Wang, S.: Anthropogenic emissions dominate ozone production in a high-elevation and highly forested region in central China: implications on forest ecosystems and regional air quality, ESS Open Active, doi:10.1002/essoar.10504327.1, 2020.

[9] Zhang, Y., Ju, T., Shi, Y., Wang, Q., Li, F., and Zhang, G.: Analysis of spatiotemporal variation of formaldehyde column concentration in Qinghai-Tibet Plateau and its influencing factors, Environ. Sci. Pollut. Res., 28, 55233-55251, doi:10.1007/s11356-021-14719-3, 2021.

[10] Wang, J., Zhang, Y., Zhang, C., Wang, Y., Zhou, J., Whalley, L. K., Slater, E. J., Dyson, J. E., Xu, W., Cheng, P., Han, B., Wang, L., Yu, X., Wang, Y., Woodward-Massey, R., Lin, W., Zhao, W., Zeng, L., Ma, Z., Heard, D. E., and Ye, C.: Validating HONO as an intermediate tracer of the external cycling of reactive nitrogen in the background atmosphere, Environ. Sci. Technol., 57, 5474-5484, doi:10.1021/acs.est.2c06731, 2023.

[11] Sörgel, M., Regelin, E., Bozem, H., Diesch, J. M., Drewnick, F., Fischer, H., Harder,

H., Held, A., Hosaynali-Beygi, Z., Martinez, M., and Zetzsch, C.: Quantification of the unknown HONO daytime source and its relation to NO_2, Atmos. Chem. Phys., 11, 20, 10433-10447, doi:105194/acp-11-10433-2011, 2011.
[12] Wang, Y., Apituley, A., Bais, A., Beirle, S., Benavent, N., Borovski, A., Bruchkouski, I., Chan, K. L., Donner, S., Drosoglou, T., Finkenzeller, H., Friedrich, M. M., Friess, U., Garcia-Nieto, D., Gomez-Martin, L., Hendrick, F., Hilboll A., Jin, J., Johnston, P., Koenig, T. K., Kreher, K., Kumar, V., Kyuberis, A., Lampel. J., Liu, C., Liu, H., Ma, J., Polyansky, O. L., Postylyakov, O., Querel, R., Saiz-Lopez, A., Schmitt, S., Tian, X., Tirpitz, J-L., Van Roozendael, M., Volkamer, R., Wang, Z., Xie, P., Xing, C., Xu, J., Yela, M., Zhang, C., and Wagner, T.: Inter-comparison of MAX-DOAS measurements of tropospheric HONO slant column densities and vertical profiles during the CINDI-2 campaign, Atmos. Meas. Tech., 13, 5087-5116, doi:10.5194/amt-13-5087-2020, 2020.
[13] Friess, U., Beirle, S., Bonilla, L. A., Bosch, T., Friedrich, M. M., Hendrick, F., Piters, A., Richter, A., van Roozendael, M., Rozanov, V. V., Spinei, E., Tirpitz, J-L., Vlemmix, T., Wagner, T., and Wang, Y.: Intercomparison of MAX-DOAS vertical profile retrieval algorithms: studies using synthetic data, Atmos. Meas. Tech., 12, 2155-2181, doi:10.5194/amt-12-2155-2019, 2019.
[14] Bosch, T., Rozanov, V., Richter, A., Peters, E., Rozanov, A., Wittrock, F., Merlaud, A., Lampel, J., Schmitt, S., de Hajj, M., Berkhout, S., Henzing, B., Apituley, A., den Hoed, M., Vonk, J., Tiefengraber, M., Muller, M., and Burrows, J. P.: BOREAS-a new MAX-DOAS profile retrieval algorithm for aerosols and trace gases, Atmos. Meas. Tech., 11, 6833-6859, doi:105194/amt-11-6833-2018, 2018.
[15] Aliwell, S. R., Van Roozendael, M., Johnston, P. V., Richter, A., Wagner, T., Arlander, D. W., Burrows, J. P., Fish, D. J., Jones, R. L., Tørnkvist, K. K., Lambert, J. C., Pfeilsticker, K., and Pundt, I.: Analysis for BrO in zenith-sky spectra: an intercomparison exercise for analysis improvement, J. Geophys. Res., 107, ACH 10-1–ACH 10-20, https://doi.org/10.1029/2001JD000329, 2002.
[16] Vandaele, A. C., Hermans, C., Simon, P. C., Carleer, M., Colin, R., Fally, S., Mérienne, M. F., Jenouvrier, A., and Coquart, B.: Measurements of the NO_2 absorption cross section from 42000 cm^{-1} to 10000 cm^{-1} (238–1000nm) at 220 K and 294 K, J. Quant. Spectrosc. Ra., 59, 171–184, 1998.
[17] Meller, R. and Moortgat, G. K.: Temperature dependence of the absorption cross sections of formaldehyde between 223 and 323 K in the wavelength range 225–375 nm, J. Geophys. Res., 105, 7089–7101, 2000.
[18] Volkamer, R., Spietz, P., Burrows, J., Platt, U.: High-resolution absorption cross-section of glyoxal in the UV-vis and IR spectral ranges, J. Photochem. Photobiol. A Chem., 172, 35–46, 2005.
[19] Rothman, L. S., Gordon, I. E., Barbe, A., Benner, D. C., Bernath, P. E., Birk, M., Boudon, V., Brown, L. R., Campargue, A., Champion, J. P., Chance, K., Coudert, L. H., Dana, V., Devi, V. M., Fally, S., Flaud, J. M., Gamache, R. R., Goldman, A., Jacquemart, D., Kleiner, I., Lacome, N., Lafferty, W. J., Mandin, J. Y., Massie, S. T., Mikhailenko, S. N., Miller, C. E., Moazzen-Ahmadi, N., Naumenko, O. V., Nikitin, A. V., Orphal, J., Perevalov, V. I., Perrin, A., Predoi-Cross, A., Rinsland, C. P., Rotger, M., Simeckova,

M., Smith, M. A. H., Sung, K., Tashkun, S. A., Tennyson, J., Toth, R. A., Vandaele, A. C., Vander Auwera, J.: The HITRAN 2008 molecular spectroscopic database, J. Quant. Spectrosc. Radiat. Transf., 110, 533–572, 2009.
[20] Fleischmann, O. C., Hartmann, M., Burrows, J. P., and Orphal, J.: New ultraviolet absorption cross-sections of BrO at atmospheric temperatures measured by time-windowing Fourier transform spectroscopy, J. Photoch. Photobio. A, 168, 117–132, 2004.
[21] Ryu, Y-H., Hodzic, A., Descombes, G., Hall, S., Minnis, P., Spangenberg, D., Ullmann, K., and Madronich, S.: Improved modeling of cloudy-sky actinic flux using satellite cloud retrievals, Geophys. Res. Lett., 44, 1592-1600, doi:10.1002/2016GL071892, 2017.
[22] Badosa, J., Gonzalez, J-A., and Calbo, J.: Using a parameterization of a radiative transfer model to build high-resolution maps of typical clear-sky UV index in Catalonia, Spain, Journal of Applied Meteorology, 789-803, 2005.
[23] Koepke, P., Bais, A., Balis, D., Buchwitz, M., De Backer, H., de Cabo, X., Eckert, P., Eriksen, P., Gillotay, D., Heikkila, A., Koakela, T., Lepeta, B., Litynska, Z., Lorente, J., Mayer, B., Renaud, A., Ruggaber, A., Schauberger, G., Seckmeyer, G., Seifert, P., Schmalwieser, A., Schwander, H., Vanicek, K., and Weber, M.: Comparison of models used for UV index calculations, Photochemistry and photobiology, 67, 657-662, 1998.
[24] Palancar, G. G., Lefer, B. L., Hall, S. R., Shaw, W. J., Corr, C. A., Herndon, S. C., Slusser, J. R., and Madronich, S.: Effect of aerosols and NO2 concentration on ultraviolet actinic flux near Mexico city during MILAGRO: measurements and model calculations, Atmos. Chem. Phys., 13, 1011-1022, doi:10.5194/acp-13-1011-2013, 2013.
[25] Xia, X., Zong, X., Cong, Z., Chen, H., Kang, S., and Wang, P.: Baseline continental aerosol over the central Tibetan plateau and a case study of aerosol transport from South Asia, Atmos. Environ., 45, 7370-7378, doi: 10.1016/j.atmosenv.2011.07.067, 2011.
[26] Xing, C., Liu, C., Wang, S., Hu, Q., Liu, H., Tan, W., Zhang, W., Li, B., and Liu, J.: A new method to determine the aerosol optical properties from multiple-wavelength O_4 absorptions by MAX-DOAS observation, Atmos. Meas. Tech., 12, 3289-3302, doi:10.5194/amt-12-3289-2019, 2019.